

Online Research @ Cardiff

This is an Open Access document downloaded from ORCA, Cardiff University's institutional repository: <https://orca.cardiff.ac.uk/id/eprint/135976/>

This is the author's version of a work that was submitted to / accepted for publication.

Citation for final published version:

Hawkings, Jon R., Skidmore, Mark L., Wadham, Jemma L., Priscu, John C., Morton, Peter L., Hatton, Jade E., Gardner, Christopher B., Kohler, Tyler J., Stibal, Marek, Bagshaw, Elizabeth A. ORCID: <https://orcid.org/0000-0001-8392-1750>, Steigmeyer, August, Barker, Joel, Dore, John E., Lyons, W. Berry, Tyanter, Martyn, Spencer, Robert G. M. and SALSA Science Team, . 2020. Enhanced trace element mobilization by Earth's ice sheets. Proceedings of the National Academy of Sciences 117 (50) , pp. 31648-31659. 10.1073/pnas.2014378117 file

Publishers page: <http://dx.doi.org/10.1073/pnas.2014378117>
<<http://dx.doi.org/10.1073/pnas.2014378117>>

Please note:

Changes made as a result of publishing processes such as copy-editing, formatting and page numbers may not be reflected in this version. For the definitive version of this publication, please refer to the published source. You are advised to consult the publisher's version if you wish to cite this paper.

This version is being made available in accordance with publisher policies.

See

<http://orca.cf.ac.uk/policies.html> for usage policies. Copyright and moral rights for publications made available in ORCA are retained by the copyright holders.



1 **Enhanced trace element mobilization by Earth's ice sheets**

2 **Jon R. Hawkings^{1,2*}, Mark L. Skidmore³, Jemma L. Wadham⁴, John C. Priscu⁵, Peter L.**
3 **Morton¹, Jade E. Hatton⁶, Christopher B. Gardner⁷, Tyler J. Kohler⁸, Marek Stibal⁹,**
4 **Elizabeth A. Bagshaw¹⁰, August Steigmeyer³, Joel Barker¹¹, John E. Dore⁵, W. Berry**
5 **Lyons⁷, Martyn Tranter⁴, Robert G. M. Spencer¹ and the SALSA Science Team**

6 *¹ National High Magnetic Field Laboratory Geochemistry Group and Department of Earth,*
7 *Ocean and Atmospheric Sciences, Florida State University, USA*

8 *² German Research Centre for Geosciences GFZ, Potsdam, Germany*

9 *³ Department of Earth Sciences, Montana State University, USA*

10 *⁴ School of Geographical Sciences, University of Bristol, UK*

11 *⁵ Department of Land Resources and Environmental Sciences, Montana State University, USA*

12 *⁶ School of Earth Sciences, University of Bristol, UK*

13 *⁷ School of Earth Sciences, Byrd Polar and Climate Research Center, The Ohio State University,*
14 *USA*

15 *⁸ Stream Biofilm and Ecosystem Research Laboratory, School of Architecture, Civil and*
16 *Environmental Engineering, École Polytechnique Fédérale de Lausanne, Lausanne, Switzerland*

17 *⁹ Department of Ecology, Faculty of Science, Charles University, Prague, Czechia*

18 *¹⁰ School of Earth and Ocean Sciences, Cardiff University, Main Building, Park Place, Cardiff,*
19 *UK*

20 *¹¹ Department of Earth and Environmental Sciences, University of Minnesota, USA*

21 ** Corresponding author Dr. Jon R. Hawkings (jhawkings@fsu.edu).*

22 **Classification:** Physical Sciences; Earth, Atmospheric and Planetary Sciences

23 **Abstract**

24 Trace elements sustain biological productivity, yet the significance of trace element mobilization
25 and export in subglacial runoff from ice sheets is poorly constrained at present. Here we present
26 size-fractionated (0.02, 0.22 and 0.45 μm) concentrations of trace elements in subglacial waters
27 from the Greenland Ice Sheet (GrIS) and the Antarctic Ice Sheet (AIS). Concentrations of
28 immobile trace elements (e.g., Al, Fe, Ti) far exceed global riverine and open ocean mean values
29 and highlight the importance of subglacial aluminosilicate mineral weathering and lack of
30 retention of these species in sediments. Concentrations are higher from the AIS than the GrIS,
31 highlighting the geochemical consequences of prolonged water residence times and hydrological
32 isolation that characterize the former. The enrichment of trace elements (e.g., Co, Fe, Mn and
33 Zn) in subglacial meltwaters compared to seawater and typical riverine systems, together with
34 the likely sensitivity to future ice sheet melting, suggests that their export in glacial runoff is
35 likely to be important for biological productivity. For example, our dissolved Fe concentration
36 (20,900 nM) and associated flux values ($1.4 \text{ Gmol year}^{-1}$) from AIS to the Fe-deplete Southern
37 Ocean exceed most previous estimates by an order of magnitude. The ultimate fate of these
38 micronutrients will depend on the reactivity of the dominant colloidal size fraction (likely
39 controlled by nanoparticulate Al and Fe (oxyhydr)oxide minerals) and estuarine processing. We
40 contend that ice sheets create highly geochemically reactive particulates in subglacial
41 environments, which play a key role in trace elemental cycles, with potentially important
42 consequences for global carbon cycling.

43 **Significance statement**

44 Trace elements are integral to biogeochemical processes at the Earth's surface and play an
45 important role in the carbon cycle as micronutrients to support biological productivity. We
46 present new data from the Greenland and Antarctic ice sheets to demonstrate the importance of
47 subglacial biogeochemical processes in mobilizing substantial quantities of these elements.
48 Usually immobile elements are found in subglacial meltwaters at elevated concentrations
49 compared to typical rivers, with most exhibiting distinctive size fractionation due to adsorption
50 onto nanoparticles. Our findings suggest that ice sheets need to be included in models of global
51 biogeochemical cycles of trace elements and studies of the fertilization of adjacent marine
52 systems, especially the Southern Ocean, due to large export fluxes of micronutrients, most
53 notably iron.

54 **1. Introduction**

55 Ice sheets cover almost 10 % of Earth's land surface area at present, up to 30 % during the last
56 glacial maximum, and account for ~ 99 % of land ice mass, yet relatively little is known about
57 the biogeochemical conditions beneath them and their importance in polar biogeochemical
58 cycles (1). Both the Greenland Ice Sheet and Antarctic Ice Sheet (GrIS and AIS respectively) are
59 undergoing rapid change due to the disproportionate impact of climatic warming in the polar
60 regions, with annual runoff and solid ice discharge contributing ~ 1 mm of sea level rise
61 equivalent per year over the last decade (2, 3). Extensive subglacial hydrological networks exist
62 beneath both ice sheets, including saturated sediments, distributed and channelized water flow
63 paths ("rivers" under ice), and interconnected subglacial lakes that drain into the ocean (4-8).
64 These subglacial hydrological systems support elevated rates of biogeochemical weathering
65 relative to global riverine values (9, 10). High elemental yields from glacial catchments are
66 thought to be sustained by an abundant supply of highly reactive comminuted rock flour with
67 reactive mineral surfaces, produced from high physical erosion rates and elevated rock:water
68 ratios at the ice-rock/sediment interface (11, 12).

69

70 Ice sheet subglacial meltwaters have recently been identified as important sources of reactive
71 sediment, solute and nutrients to downstream ecosystems (13-16), highlighting a potentially
72 important, yet poorly understood contribution to global carbon cycling (1). The majority of
73 samples have been collected from comparatively accessible glacial field sites, with extremely
74 limited data available from Antarctic subglacial environments due to extreme technological and
75 logistical challenges of access (17, 18). Given the paucity of data, we do not understand the

76 implications of changing ice sheet melt for biogeochemical cycling in the polar regions, and their
77 impact on local and regional processes (19).

78
79 Trace element (TE; elements present at low “dissolved” concentrations in natural waters,
80 operationally usually < 50 ppb) concentrations in glacial meltwaters have received minor
81 attention to date (15, 20, 21). The concentration and speciation of TEs may provide important
82 information about the chemical weathering environment, redox processes, water sources, and
83 subglacial hydrological pathways that are not always apparent using only major ion chemistry
84 (22-24), although the source, speciation, transformation and co-association of many trace
85 elements are still not well understood. For example, Al and V (and to a lesser degree Ba) can be
86 used as tracers of silicate weathering intensity (25), Mo, Cd and Zn are strongly chalcophilic
87 elements and their presence is indicative of oxidation of sulfide minerals (26, 27), and Fe and Mn
88 are redox sensitive and therefore their presence and speciation indicate reducing source waters
89 and elucidates oxidation rates (28). A number of TEs (e.g. Ni, Co, Pb and Cr) are siderophiles
90 and therefore their mobility can provide information of weathering, transport and form of Fe,
91 and, by association, biologically mediated redox processes (29). U can be used as a tracer of
92 oxidative weathering and is sourced mainly from sedimentary rocks (30), while Sr
93 concentrations can be an excellent indicator of carbonate mineral weathering (31). Furthermore,
94 many TEs are biologically essential micronutrients that play critical roles in cellular processes,
95 including C, N and P transport and assimilation, and as components of metabolic co-
96 enzymes/metalloproteins (e.g., Fe, Mn, Mo, Co, Zn, Cu, Cd, Mo, V; (32-34)). Consequently their
97 export from ice sheets to downstream ecosystems can have important implications for biological
98 productivity and associated patterns of nutrient limitation and elemental inventories (15, 35, 36).

99 We hypothesize that ice sheets play an important yet poorly constrained role in TE cycling given
100 the elevated chemical erosion rates under large ice masses (9, 37, 38), the unique biogeochemical
101 weathering environment (Table S1) in subglacial hydrological systems and the large and
102 increasing ice sheet freshwater export. Constraining TE export from ice sheets is critical for
103 understanding downstream elemental cycling and associated ecosystem response, and the
104 implications of future changes to glacial meltwater discharge.

105
106 We present size-fractionated TE concentration data ($< 0.02 \mu\text{m}$, “soluble”, s[element]; < 0.45 ,
107 “dissolved”, d[element]; $0.02 - 0.45 \mu\text{m}$, “colloidal/nanoparticulate”, cn[element]) for subglacial
108 meltwaters sampled beneath the Antarctic (Mercer Subglacial Lake; SLM; a hydrologically-
109 active subglacial lake) and emerging from the Greenland (Leverett Glacier; LG; a large ice sheet
110 catchment) ice sheets (Fig. 1). We use these data to (i) examine how biogeochemical weathering
111 processes and water sources influence the TE geochemistry of the subglacial environment and
112 infer the potential significance of glacially derived TEs to downstream ecosystems surrounding
113 ice sheets, (ii) determine the magnitude of colloidal/nanoparticulate phases for the majority of
114 TEs measured, and (iii) assess the enrichment/depletion of micronutrients in glacial meltwaters
115 compared to global non-glacial riverine mean values (hereafter referred to as “riverine mean
116 values”) and typical seawater concentrations. Our results significantly advance the understanding
117 of biogeochemical processes beneath large ice sheets and highlight the potential importance of
118 meltwaters in global TE inventories.

119

120 **2. Results and discussion**

121 **2.1 Controls on trace element composition of AIS and GrIS meltwaters**

122 Elemental concentrations in SLM and LG waters span an extremely large range with clear
123 patterns of size fractionation in the “dissolved” <0.45 μm phase (dTE; Figs. 2 and 3, Table S1).
124 Data from both locations indicate that the dominant dTE in subglacial meltwaters are those
125 typically associated with lithogenic weathering of the more abundant elements in the Earth’s
126 crust and oxyhydroxide mineral phases, i.e., dAl, dFe and dTi, with concentrations higher than
127 the mean of non-glacial rivers (Fig. 2b, Table S1). For example, dFe concentrations in LG and
128 SLM were up to an order of magnitude higher than mean riverine waters (2,390 and 20,900 nM
129 compared to 1,180 nM), dTi concentrations were at least one order of magnitude higher (277 and
130 2,080 nM in LG and SLM waters respectively, compared to ~ 10 nM riverine mean), and dAl
131 concentrations at LG and SLM (351 – 105,000 nM) are similar only to concentrations reported in
132 GrIS meltwaters (300 – 13,600 nM, (21)). The elevated concentrations of typically less mobile
133 elements point to the influence of biogeochemical weathering processes in waters with a high pH
134 (up to 9.6 at LG and 8.2 at SLM; Table S1). The high concentrations of these elements also
135 reflect the importance of physical weathering processes generating an abundant supply of
136 microparticles and predominance of refractory primary minerals and nanoparticulate
137 (oxyhydr)oxides, as observed previously in glacial meltwaters (23, 39, 40), despite the low
138 temperatures (~ 0 °C) commonly associated with suppressed weathering rates. These weathering
139 processes hold even within SLM where subglacial water residence times are prolonged (\sim years;
140 (41)), underlying sediments are of contrasting origin (overridden marine sediments vs freshly
141 crushed shield bedrock), and suspended sediment concentrations are relatively low (~ 20 mg L⁻¹
142 at SLM vs $\sim 1,000$ mg L⁻¹ at LG), indicating lower local physical erosion rates and turbulence.
143

144 The predominant driver of TE composition in these subglacial systems appears to be the
145 weathering of silicate minerals, as elucidated from the abundance of TEs commonly sourced
146 from silicate weathering. For example, Vanadium (V) is almost entirely derived from silicate
147 weathering (25) and concentrations in ice sheet meltwaters exceeded the riverine mean value
148 (~14 nM) (24, 25), with LG waters more than twice as concentrated on average (dV 31.1 nM, up
149 to 89.2 nM) and SLM waters more than an order of magnitude higher (dV 265 nM; Fig. 3, Table
150 S1). This contrasts with more variable dissolved silicon (Si) concentrations, which are low in LG
151 waters (9.2 – 56.9 μM ; (42)), with Si likely retained in secondary weathering products (43) while
152 V is not, yet similar to global riverine concentrations of ~158 μM in SLM (120 – 140 μM ; Fig.
153 2) (44). Other trace elements typically associated with silicate weathering and at much higher
154 abundance in silicate rocks than carbonate rocks are also found at high concentrations in
155 meltwaters from both ice sheets, especially Al, Ti, Co, Cr and Ni (Fig. 2b) (45).

156

157 The major ion chemistry of Whillans Subglacial Lake (SLW) adjacent to SLM (Fig. 1; (38)), and
158 from GrIS (9, 16, 37, 42) is also consistent with enhanced silicate mineral weathering beneath ice
159 sheets (46). This contrasts older views that silicate mineral weathering was insignificant beneath
160 glacial systems as valley glaciers typically exhibit geochemical signatures of carbonate
161 weathering (9, 12). The principal weathering conditions are likely to be different at the two ice
162 sheet locations. We contend that GrIS waters exhibit silicate weathering signatures because the
163 underlying bedrock is either carbonate poor (37, 47) and/or that meltwater residence times are
164 prolonged in larger GrIS catchments (42) enhancing weathering of minerals with slower
165 dissolution kinetics. The high pH of LG meltwaters (up to 9.6) also enhances the solubility of
166 primary aluminosilicate minerals (12). AIS meltwaters exhibit geochemical conditions of waters

167 with long residence times and highly weathered sediments, where reactive minerals have been
168 previously weathered from the rock matrix (38), and where porewaters in the subglacial
169 sediments are likely to provide a concentrated source of solute to waters via diffusion (38).

170

171 Sr concentrations in LG and SLM meltwaters reinforce this interpretation. Sr is found at high
172 concentrations in carbonate minerals, with Sr^{2+} substituting for Ca^{2+} , and is therefore common in
173 limestones, dolostones and evaporites. Concentrations of Sr in LG meltwaters are low (51.6 nM;
174 Fig. 2a, Table S1), consistent with previous measurements (47). SLM Sr concentrations are
175 similar to the riverine mean (~ 850 nM vs 600 – 900 nM; Figs. 2 and 3; (31)) but much lower
176 than riverine catchments where carbonate/evaporitic weathering dominates (e.g., the Colorado
177 River, $\sim 10,000$ nM, Rhone and Rhine River's, $\sim 6,000$ nM, and the Mekong River, $\sim 3,000$ nM;
178 (31)).

179

180 Weathering of sulfide minerals also appears to contribute to meltwater TE composition (38).
181 High cnFe and SO_4 concentrations in all samples indicate iron sulfide oxidation may be an
182 important weathering pathway for generation of Fe oxyhydroxide nanoparticle aggregates 0.02-
183 $0.45 \mu\text{m}$ in size (Fig. 2) (23, 48). The importance of sulfide mineral weathering is reinforced
184 from Mo, a strongly chalcophilic element preferentially weathered from sulfide minerals
185 (predominantly pyrite; (26)). Mo concentrations in LG (1.9 – 11.3 nM) are similar to the global
186 riverine mean (8 nM; (26)) and are substantially higher in SLM (52.9 nM; Figs. 2 and 3).

187

188 **2.2 The colloidal world of subglacial environments**

189 At least 14 of the 17 elements measured have a colloidal/nanoparticulate (cn) component in
190 glacial meltwaters (Table S1, Fig. 3). TEs can be broadly separated into three operationally
191 defined classifications (Fig. 3): (Group 1) those strongly associated with the cn phase (>75% cn);
192 (Group 2) those moderately associated with the cn phase, but with a significant soluble fraction
193 ($\geq 25\%$ but $\leq 75\%$ cn); and (Group 3) elements predominantly associated with the soluble phase
194 (<25% cn). SLM and LG meltwaters share nine common Group 1 elements: Ti, Fe, Pb, Co, Ni,
195 Ba, Al, Zn and Cu; two common Group 2 elements: Cd and V; and three common Group 3
196 elements: Li, Sr and Mo. Cr is found mainly in the colloidal phase at both locations but in Group
197 1 for LG and Group 2 for SLM. U and Mn have contrasting distributions; U is in Group 1 for LG
198 and Group 3 for SLM, while Mn is a Group 1 element at SLM only found in colloidal size
199 fractions, compared to Group 2 at LG, with a substantial proportion (>33%) present as sMn.

200
201 Most elements fall into Group 1 in both ice sheet environments (Fig. 3). This phase is likely to
202 consist mostly of inorganic material since dissolved organic carbon (DOC) concentrations are
203 very low at both SLM and LG sampling locations ($\sim 30 \mu\text{M}$, Table S1; (49)). The large
204 concentrations and proportions of Fe and Al in the cn size fraction (cnFe = 2,390 nM at LG and
205 20,900 nM at SLM; cnAl = 14,200 nM at LG and 65,000 nM at SLM, Fig. 2 and 3) indicate that
206 Fe oxyhydroxide nanoparticles (likely ferrihydrite, goethite and hematite) and Al oxyhydroxide
207 nanoparticles (likely poorly crystalline alumina or gibbsite) control the speciation of these
208 elements via their large adsorption capacity, surface precipitation or coprecipitation (50).

209 Elements that have an affinity with oxyhydroxide minerals (e.g., Cr, Co, Zn, Ni, Pb via binding
210 to -OH functional groups; (29, 51)), especially just below the oxyhydroxide zero point of charge
211 (pH ~ 9 for Fe oxyhydroxides), are present at much lower concentrations in the soluble phase

212 (<20 % of dTE; Fig. 3). A large sorption capacity of colloidal material for other trace elements is
213 also observed in large non-glacial riverine systems, although not to the same degree (51).

214

215 The unique features of subglacial weathering environments provide an explanation for the
216 predominance of these colloidal/nanoparticulate TE phases. The low temperatures ($\sim 0\text{ }^{\circ}\text{C}$) may
217 aid in slowing the aggregation and aging of nanoparticles into denser, larger size fractions >0.45
218 μm in size, with smaller aggregates having a greater adsorption capacity due to their extremely
219 high surface area to volume ratios (52). Additionally, aggregation under higher pH conditions
220 (mean pH was >8 , up to 9.6; Table S1) has been found to generate less ordered porous
221 aggregates with high sorption properties (53).

222

223 It is possible that other mechanisms inducing this size fractionation are important. Nanoclays
224 rich in Al and Fe (e.g., allophane) can also adsorb/incorporate less abundant elements (54).

225 Alternatively, the extremely fine size fraction of comminuted sediments allow crushed primary
226 rock material to pass through larger pore size filter membranes (55), and thus this phase is more
227 indicative of a weathered bulk bedrock signature (i.e., mobile elements have been leached,
228 leaving relatively immobile elements). It is likely this process would differ for SLM (long
229 residence time) versus LG (comparatively short residence time), with aged secondary minerals
230 (e.g., nanoclays) dominating in the former and primary minerals, or freshly precipitated
231 secondary minerals (e.g., amorphous iron oxyhydroxides) dominating in the latter.

232

233 The consideration of the cn size fractions appears to be critical in determining the behavior and
234 concentration of filterable TEs in subglacial meltwaters. For example, the operationally defined

235 filter membrane pore size cut off has a substantial impact on the observed concentration of TEs
236 in SLM (Fig. 3). In addition to 0.02 and 0.45 μm , 0.22 μm filtered samples were taken from
237 SLM allowing partitioning between small (0.02 - 0.22 μm ; cn^{small}) and large (0.22 - 0.45 μm ;
238 cn^{large}) cn species. These data show that colloidal/nanoparticulate phases were more abundant in
239 the larger size fraction. In particular, < 10 % of cnTi and cnFe is contained in the cn^{small} phase
240 compared to > 90 % in the cn^{large} phase. The geomicrobiological implications of this partitioning
241 are uncertain as the reactivity of this material is not well understood. Given the very high surface
242 area to volume ratios of these particles, we hypothesize they are highly reactive but likely require
243 more complex and energy intensive processing before biological uptake. The large difference in
244 concentration between colloidal size fractions likely reflects the aggregation of nanoparticulate
245 material to features >0.2 μm , as observed in high resolution photomicrographs of glacial
246 suspended sediments (23, 39).

247

248 **2.3 Contrasting trace element cycling under ice sheets**

249 Several broad similarities exist in the TE composition of SLM and LG meltwaters despite the
250 contrasting hydrological, geological and geochemical conditions. Most TEs appear to have a
251 colloidal/nanoparticulate component, as discussed above. Only Sr, Mo and Li existed
252 predominantly in the soluble phase in both environments likely because they are highly mobile
253 elements (particularly Sr and Mo) with geochemical behavior similar to other alkaline and
254 alkaline-earth cations (Fig. 3 and 4). Additionally, the presence of sMo at similar or elevated
255 concentrations to riverine waters at both field sites also implies contributions from an oxic
256 weathering environment (likely alongside flushing of hypoxic/anoxic stored waters under LG)
257 (26), which is reinforced by mean dissolved O_2 saturation exceeding 100 % (with respect to

258 atmospheric O₂) at both sampling sites (Table S1; (56)). Subglacial concentrations of dissolved
259 lithogenic TEs associated with the most abundant crustal elements are also high in both
260 meltwaters, as previously discussed.

261
262 Several key differences exist between the subglacial meltwaters sampled despite these broad
263 similarities. The major difference between subglacial meltwaters in SLM and emerging from LG
264 is the absolute elemental concentration. Both cnTE and sTE concentrations in SLM meltwaters
265 are generally much higher than in LG meltwaters (up to an order of magnitude; Table S1, Fig.
266 2c). High concentrations of dTE in AIS subglacial environments have been hypothesized (57)
267 given the long residence time of AIS meltwaters, inputs of solute from underlying sediments
268 (38), no subglacial meltwater dilution from surface meltwater (as with the GrIS)(13, 42), and
269 elevated macronutrient concentrations in SLW (15), but has been supported by little evidence
270 until now. Contrasting hydrological environments are also reflected in the mean specific
271 conductance of meltwaters (a proxy for solute concentration), which differ by more than an order
272 of magnitude (12.6 vs 272 $\mu\text{S cm}^{-1}$; Table S1), as well as differences in major ion composition
273 (9, 38, 42). These differences also highlight the distinct biogeochemical processes occurring
274 beneath ice sheets. Enhanced silicate weathering in long residence time AIS meltwaters produces
275 an abundance of clay minerals and the potential for surficial ion exchange on these clay minerals
276 in long residence time AIS meltwaters (38). This contrasts with shorter residence times of GrIS
277 meltwaters with rapid silicate hydrolysis and carbonation reactions on freshly crushed primary
278 rock minerals (42), and substantial dilution by incoming fresh supraglacial meltwaters.

279

280 The speciation of two trace elements highlights some of the variation between ice sheet
281 environments: U (100 % sU in AIS, but < 1 % sU in GrIS) and Mn (< 1 % sMn in AIS, but > 35
282 % sMn in GrIS). This contrasting behavior is somewhat surprising given the broad similarities
283 observed between other TEs. The behavior of U may relate to the sediment source, with SLM
284 underlain by overridden marine sediments (with U commonly enriched in sedimentary
285 environments (30)), versus LG sediments generated from the Precambrian shield silicate
286 bedrock, likely to be depleted in U (24, 30). SLM waters are also highly enriched in U compared
287 to mean riverine values (29.7 nM vs 0.78 nM; (30); Table S1). Predominance of cnU phases in
288 LG meltwaters may be linked to adsorption onto nanoparticulate Fe oxyhydroxides (58).
289 Evidence of this is given by the lower cnFe:cnU ratio, < 5,000, relative to the Fe:U upper
290 continental crust ratio of shield bedrock, ~ 15,000 (45). No U is associated with the cn fraction at
291 SLM, possibly due to stabilization by ligands (e.g., as $[\text{UO}_2(\text{CO}_3)_3]^{4+}$ (59)) or reflecting the
292 contrasting transport processes (likely grinding of primary rock particles and turbulent water
293 flow at LG versus diffusion from sediments in SLM).

294

295 The absence of sMn in SLM waters versus LG meltwaters is likely indicative of the longer water
296 residence times (~years; (41)) combined with oxidative weathering environment (>100 % O₂
297 saturation with respect to atmospheric O₂; Table S1). The lack of sMn in SLM waters indicates
298 almost complete oxidation of soluble Mn²⁺ species to insoluble Mn^{3+/4+}, and/or adsorption of
299 Mn²⁺ to Mn oxyhydroxides or clays (60). Conversely, in GrIS catchments meltwater transport
300 times through the subglacial drainage systems to the meltwater portal are comparatively rapid
301 (hours to weeks (61)). Furthermore, isolated hypoxic and anoxic subglacial environments present
302 underneath the GrIS (62) are favorable for generating high point concentrations of sMn (via Mn

303 reduction) and allow persistence of Mn^{2+} despite meltwater being fully oxygenated upon
304 sampling. The half-life of Mn^{2+} in oxygenated waters, before oxidation to Mn^{3+}/Mn^{4+} and
305 precipitation as Mn oxides, is significantly longer than Fe^{2+} in the absence of stabilizing ligands
306 (hours to weeks versus seconds to minutes (63)), especially at low temperatures, and it appears
307 soluble Mn^{2+} species persist during transport in the LG subglacial system where stored
308 anoxic/hypoxic subglacial waters are mixed with oxygenated surface meltwater.

309

310 TE mobility can also help explain differences between SLM (AIS) and LG (GrIS) chemical
311 weathering environments. Elemental mobility was estimated via a first order approach (22) by
312 normalization of dissolved concentrations to mean upper continental crust composition (45) and
313 then normalizing to the resulting Na rock:solution ratio so that Na = 1 (“mobility index” - MI).
314 Our data indicate comparatively low mobility of TE in SLM meltwaters versus relatively high
315 mobility in LG meltwaters compared to non-glacial rivers (Fig. 4). Highly chemically weathered
316 “bleached” sediments underlie SLM, with less mobile elements (MI <1; Fig. 4b) more likely
317 incorporated into secondary weathering products, likely clay minerals >0.45 μm in size via
318 adsorption/ion exchange and/or co-precipitation (38, 64), with highly mobile elements (MI >1;
319 Figure 4a) retained in solution. In contrast, typically less mobile elements (MI < 1) generally
320 have higher mobility in LG meltwaters than both SLM and mean riverine waters, likely
321 reflecting hydrolysis of primary rock minerals after comminution (42).

322

323 Finally, LG meltwaters exhibit large variability in TE concentrations driven by seasonal changes
324 in the subglacial drainage system in response to surface meltwater forcing (42, 61, 65). It is
325 currently unknown if there is substantial temporal variation in meltwater composition in SLM or

326 under AIS more widely. Any TE geochemical variability in SLM would be likely to reflect
327 drain/refill cycles in the lake (41), the geochemical consequences of which are unknown but
328 unlikely to be as large as the variation observed in meltwater emerging from LG, given the
329 significant seasonal hydrochemical evolution of GrIS catchments (42).

330

331 **2.4 Implications for downstream biogeochemical cycling**

332 Several TE are essential micronutrients for microbiota, serving as important components of (co-)
333 enzymes and performing essential roles in cellular processes such as nitrogen and carbon fixation
334 (32). The most important trace elements for microbial metabolism are thought to be Fe, Mn, Mo,
335 Co, Zn, Cu, Ni, V and Cd (32, 33), several of which are can be limiting or co-limiting for
336 photoautotrophic and heterotrophic activity in marine (35, 66) and freshwater ecosystems (36).
337 Recently, ice sheets have been hypothesized to be significant sources of Fe to the ocean, with
338 high concentrations of dFe found in meltwaters from the GrIS (23, 48, 67, 68) and (sub)Antarctic
339 maritime islands (69, 70), as well as significant quantities of labile particulate Fe rafted in
340 icebergs (71, 72). Limited data exists for glaciated environments, apart from spot samples from
341 several Greenlandic glaciers (21) that alluded to high concentrations in meltwater. The two ice
342 sheets deliver $>2000 \text{ km}^3$ of freshwater (i.e., $>5 \%$ of the riverine freshwater flux (73)) to the
343 ocean each year and this is increasing. Therefore, a first order consideration of the associated TE
344 input is important in understanding any influence on biological productivity in polar waters
345 adjacent to the ice sheets and potential nutrient limitation/alleviation. Our discussion focuses on
346 flux estimates “at the gate” where meltwater enters the marine environment (Tables 2 and 3), but
347 we acknowledge that estuarine processing can drastically modulate the TE flux into the open
348 ocean (74, 75).

349
350 Nearly all dissolved micronutrient concentrations are elevated in glacial meltwaters from the
351 GrIS and AIS relative to mean ocean concentrations (Table S1). This contrasts with the relatively
352 low dissolved macronutrient (C, N and P) concentrations reported previously for GrIS (76, 77),
353 but is consistent with higher concentrations reported beneath AIS (Fig. 2a (15)). A notable
354 exception is Cd, which is lower in both GrIS (0.015 ± 0.019 nM) and AIS (0.21 ± 0.011 nM)
355 meltwaters comparative to non-glacial riverine waters (0.712 nM, (22)) and bulk oceanic waters
356 (0.6 nM, (78)). Cd is a highly mobile but rare chalcophilic element, so these low concentrations
357 indicate Cd-bearing sulfides (e.g., zinc sulfides rich in Cd such as sphalerite and cadmium
358 sulfides such as greenockite) are depleted in sediments underlying LG and SLM, or reflects an
359 anthropogenic source of the high dCd in rivers (27), which is absent in pristine glacial systems.
360 SLM waters are enriched in all other bioessential trace elements with concentrations of dCo,
361 dCu, dFe, dMn and dZn all more than one order of magnitude higher in SLM waters than marine
362 waters and typically exceed or are similar to mean riverine concentrations (Table S1; Fig. 2). LG
363 concentrations also exceed bulk oceanic concentrations and are broadly similar to mean riverine
364 concentrations (Table S1; Fig. 2). LG Mn concentrations appear an order of magnitude lower
365 than riverine concentrations, although they exceed bulk oceanic concentrations by more than two
366 orders of magnitude (72.6 vs 0.3 nM; Table S1). Mean riverine Mn concentrations reported also
367 appear biased by a lack of high quality riverine data and concentration estimates in the Amazon
368 River (which has a disproportionate effect on the mean concentration) that span an order of
369 magnitude (60 – 920 nM (22)). Moreover, LG dMn concentrations are similar to or exceed many
370 North American rivers (e.g., the Columbia River, ~10-100 nM, and the Mississippi, ~1-70 nM;
371 (28, 79)).

372

373 The relatively high “dissolved” micronutrient concentrations in ice sheet meltwaters that we
374 measured provide the first evidence that ice sheet meltwaters could supply a suite of dissolved
375 micronutrients to support biological production in coastal regions surrounding AIS and GrIS (80,
376 81). Collectively these large regional ice sheet micronutrient inputs should be considered in
377 future TE biogeochemical models where they are currently absent (66, 82, 83).

378

379 **2.5 Antarctic Ice Sheet fertilization of the Southern Ocean?**

380 Our data have particularly important implications for our understanding of ice sheet fertilization
381 of the Fe-deplete Southern Ocean (84). No size speciated dTE data from subglacial hydrological
382 systems beneath AIS have been previously obtained, although the enrichment of Fe in AIS
383 meltwaters compared to surrounding oceanic environments has been hypothesized and
384 previously measured at SLW (15, 23, 57, 68). The data we present indicate that meltwater
385 discharge from interconnected subglacial lake hydrological systems draining AIS into coastal
386 embayments is likely to elevate labile Fe concentrations (Fig. 2), supporting previously
387 hypothesized glacial Fe fertilization in coastal regions of the Southern Ocean (68-70, 85, 86).
388 The cnFe concentrations in SLM (20,900 nM) far exceed concentrations in LG and other GrIS
389 meltwaters (50 – 7,500 nM; Table S1; (48, 67)). AIS dFe flux estimates based on SLM
390 concentrations (0.66 – 2.1 Gmol year⁻¹; Table 1) exceed previous AIS estimates by an order of
391 magnitude (0.02 – 0.32 Gmol year⁻¹; (23, 69)) and are similar to GrIS dFe export estimates
392 despite the much lower discharge. The SLM values are also consistent with upper end AIS
393 subglacial meltwater Fe concentration estimates used in a study (30,000 nM; (87)), which
394 produced modeled data of Southern Ocean Fe and primary productivity consistent with

395 observations. Even if estuarine removal in the Siple Coast underneath the Ross Ice Shelf filters
396 99% of subglacially exported Fe, there is still potential for significant AIS Fe fertilization of
397 coastal ecosystems if these species persist and are labile. A more recent modelling study found
398 limited, more localized fertilization potential of ice shelf meltwater (88), highlighting the
399 complexities of evaluating ice sheet influence on downstream productivity. However, the
400 mechanisms of Fe delivery discussed in that study differ (ice shelf melt versus subglacial
401 meltwater discharge), meltwater concentrations used were lower, and it remains difficult to
402 disentangle meltwater (direct and indirect) vs sediment sources (argued by the authors to be more
403 important) in coastal regions where primary productivity is high. Additional field data and
404 biogeochemical modelling are clearly needed to disentangle and constrain the major sources of
405 Fe to the Southern Ocean, and the impact of direct (meltwater outflow) vs indirect (glaciogenic
406 sediments comprised in part from material deposited by meltwaters) glacial inputs.

407
408 An interesting juxtaposition exists when comparing Fe data from SLM to SLW, where the only
409 comparative concentration estimates for the AIS exist. The dFe concentrations reported for SLW
410 (15) are ~30 nM, compared to the phase size equivalent (<0.22 μm) measured in SLM of 981
411 nM. This leads to substantial variability in estimated dFe fluxes to the Siple Coast: 61 kmol year^{-1}
412 (15), compared to 40,000 kmol year^{-1} (Table S2). The Fe export calculated from SLW was
413 estimated to be able to maintain measured microbial activity in the Siple Coast region (based on
414 elemental stoichiometry (15)), therefore estimates based on SLM concentrations vastly exceed
415 that. Although filter type and pore size are not directly comparable, these differences point to the
416 possibility of substantial spatial or temporal heterogeneity (e.g., fill/drain cycles (41)) in Fe
417 concentrations beneath AIS and/or the influence of filtration artifacts such as membrane clogging

418 and reduction in effective pore size (89). Modeling studies of glacial Fe sources to the Southern
419 Ocean coupled to observations of euphotic zone dFe and chlorophyll *a* concentrations (87, 90)
420 and indirect observations under ice shelves (91) reveal that SLM may be more representative of
421 an enriched AIS subglacial endmember. We do not account for reactive particulate iron
422 concentrations in these estimates (e.g. amorphous ferrihydrite (39)), which were found to be
423 elevated in SLW (15) and are likely to be high in SLM. The potential for high spatial variability,
424 consistency in filtration methodology and elevated labile particulate Fe clearly demonstrate the
425 need for future coordinated studies on AIS subglacial environments.

426

427 **2.6 Modulating effects of estuarine processing**

428 The significance of subglacial trace micronutrients to downstream ecosystem processes will also
429 depend on their behavior following delivery. Downstream elemental transformations are likely to
430 be complex, with each micronutrient exhibiting unique geochemical characteristics during
431 mixing of freshwater with seawater that vary regionally, including conservative behavior (e.g.,
432 Ni, Cu, V and Mo), nonconservative excess (e.g., Mn, Co, Zn and Cd) and nonconservative
433 removal (e.g., Fe)(92). The behavior of individual elements will depend on multiple
434 biogeochemical factors such as organic matter concentration and composition, ligand binding,
435 benthic recycling (e.g., via diffusive porewater fluxes or sediment resuspension), desorption
436 from mineral surfaces, and microbial uptake or alteration (such as Mn oxidation) (79, 92). The
437 impact of micronutrients on downstream ecosystem processes will also depend on the physical
438 features of the downstream environment. Meltwaters from subglacial environments under the
439 AIS often flow into large sub-ice shelf cavities >400 km from the open ocean with long
440 residence times (several years in the Ross Ice Shelf cavity (15)). These sub-ice shelf

441 environments will impede immediate delivery of micronutrients to photosynthetic primary
442 producers. Nevertheless, our results (Table 1) indicate AIS subglacial meltwaters may still be
443 able to subsidize the micronutrient inventory in coastal regions of the Southern Ocean where
444 high productivity has been observed, such as pelagic regions proximal to the Ross Ice Shelf
445 downstream of Siple Coast inputs (Table S2), and other major ice streams (81). Conversely, GrIS
446 meltwaters enter coastal regions either as turbid meltwater rivers emerging from land-
447 terminating glaciers, or via injection into fjord at depth from tidewater glaciers. These two
448 delivery mechanisms have been observed to drastically alter the biogeochemical conditions for
449 primary producers and surface macronutrient concentrations, but little information is currently
450 available on micronutrient behavior in fjords (19, 80, 93).

451
452 The presence of high colloidal TE concentrations in subglacial meltwater is likely to have
453 significant implications for downstream transport and lability. These implications are especially
454 important for Fe, where $cnFe$ will aggregate, flocculate and be scavenged from the water column
455 at low salinities, with implications for TEs associated with Fe. For example, >95% of dFe is
456 removed in low salinity regions of Alaskan and Greenlandic estuaries/fjords, but high
457 concentrations still remain at seawater salinities close to the coast because of the high glacial
458 meltwater end-member concentrations (74, 75). The very high dFe concentrations observed in
459 SLM indicate potential for long distance transport of glacially derived iron even with large
460 removal rates. The bioavailability of colloidal species is also uncertain as they represent a
461 complex mixture of organic and inorganic material with varying labilities. Soluble species are
462 likely the best empirical measurement of potentially bioavailable phases, yet represent a small
463 fraction of the total dissolved pool (Fig. 3). Colloidal species of trace metals appear more

464 important than soluble species in supply and removal processes in oceanic and coastal systems
465 (94) and this will almost certainly depend on the mineralogy of the colloid/nanoparticles usually
466 included in the filterable fraction (40).

467

468 **3. Conclusions**

469 Ice sheets export globally significant quantities of trace elements in subglacial meltwaters and as
470 such should be considered an important component of polar biogeochemical cycling of trace
471 elements. Trace elements in meltwaters sampled from the Greenland and Antarctic ice sheets are
472 derived mainly from the biogeochemical weathering of silicate and sulfide minerals, consistent
473 with previous research on major ion composition and mineralogy (9, 38, 42, 43), and further
474 highlighting the potentially important role of ice sheets in enhanced silicate weathering and long
475 term carbon drawdown (46). Concentrations of trace elements in subglacial meltwaters are
476 generally high despite low temperatures, which likely reflects weathering of rock microparticles
477 and/or long water residence times in high rock:water subglacial drainage systems. The
478 importance of colloidal/nanoparticulate species depend on the element in question, but our data
479 indicate a prevalence of elemental species 0.02-0.45 μm in size compared to truly soluble (<0.02
480 μm), aqueous species. Nanoparticulate oxyhydroxide minerals are therefore important in
481 subglacial environments with a high sorption capacity and have important implications for
482 lability and the ultimate fate of trace elements in the downstream cascade. The role of subglacial
483 export of trace elements to adjacent/downstream polar ecosystems can elevate micronutrient
484 availability and therefore the carbon cycle by sustaining or altering biological productivity.
485 Downstream TE transport is especially relevant to Antarctica because biological productivity in
486 the Southern Ocean surrounding the AIS is limited by Fe (84). The significance of these fluxes

487 will depend on sub-ice shelf and estuarine processing, which are poorly quantified at present.
488 Our findings have implications for the understanding of elemental cycling during periods of
489 glacial transition, including the increasingly rapid melt of the ice sheets predicted in future
490 climate warming scenarios.

491

492

493 **4. Methods**

494 **4.1 Study areas**

495 **4.1.1 Mercer Subglacial Lake (West Antarctic Ice Sheet)**

496 AIS samples were collected in December 2018-January 2019 from Mercer Subglacial Lake
497 (SLM; Fig. 1b; 84.661°S, 149.677°W) 1,092 m beneath the surface of the West Antarctic Ice
498 Sheet. SLM is one of the largest lakes (136 km²) beneath Siple Coast ice streams and fed by
499 subglacial waters from the East and West Antarctic Ice Sheets. Approximately 25 % of its water
500 is hypothesized to be sourced from beneath the East Antarctic Ice Sheet via Mercer Ice Stream
501 (95). The lake is hydrologically active with multiple drain/fill cycles observed over the past
502 decade (41). The lake depth was 15 m at the time of sampling and the falling ice elevation
503 indicates the lake was in a draining stage (96). Modeling reveals that downstream flow is through
504 subglacial channels into a marine embayment at the southern reach of the Ross Ice Shelf cavity,
505 with episodic discharge exceeding 300 m³ sec⁻¹ during flood events (7). This region of the West
506 Antarctic Ice Sheet is underlain by glaciomarine sedimentary basins (97).

507

508 **4.1.2 Leverett Glacier (Greenland Ice Sheet)**

509 GrIS samples were collected from the proglacial river emerging from a subglacial portal exiting
510 Leverett Glacier (LG; 67.062°N, 50.201°W; Fig. 1a; (11, 13, 61)) in south-west Greenland
511 during the 2015 ablation season. LG is a polythermal-based glacial outlet of GrIS estimated to
512 drain a hydrologically active catchment area of ~600-900 km² (11), and is thought to be fairly
513 representative of GrIS land terminating catchments at large, as detailed elsewhere (13, 62). The
514 LG meltwater river feeds into a larger river system (Watson River) ~6 km downstream, which
515 discharges into Søndre Strømfjord. Bedrock geology is predominantly Precambrian Shield
516 gneiss/granite, which is the dominant geology under much of GrIS (98).

517

518 **4.2 Sample collection, processing, storage and analysis**

519 SLM water samples were retrieved using a standard 10 L Niskin bottle pre-cleaned with 1.2 M
520 HCl (followed by copious rinsing with ultra-pure water (UPW); Milli-Q; 18.2 MΩ cm⁻¹), 3 %
521 H₂O₂ and lowered through a ~0.6 m diameter borehole drilled using a microbiologically clean,
522 hot water drilling system (17, 18). A 10L Niskin bottle was retrieved in six casts into the lake
523 from 29th December 2018 to 4th January 2019. Bulk LG water runoff samples were collected by
524 hand at least once daily from 1st May to 28th July 2015 ~1 km downstream of the glacier portal to
525 capture changes in subglacial hydrology (65) as detailed below.

526

527 **4.2.1 TE sampling, processing and storage**

528 Samples for TE analysis were collected cleanly according to strict size-fractionated trace element
529 protocols ((23, 89); procedural blanks detailed in Table S3). All sampling equipment (250 mL
530 and 15 mL Nalgene® LDPE bottles, and PP/PE syringes) were cleaned sequentially in 1%
531 DECON (overnight), 6 M HCl (48 hours) and 3 M HNO₃ (48 hours), with copious rinsing in

532 UPW in between washes, and final drying in a laminar flow hood (ISO 5). Whatman® GD/XP
533 PES (polyethersulfone) 0.45 µm, Millex-GP Millipore Express 0.22 µm (PES; only SLM) and
534 Whatman® Anotop 25 0.02 µm syringe filters were cleaned with ultra-trace metal grade HCl
535 (Optima™). The 0.22 and 0.45 µm syringe filters were cleaned by passing through 20 mL of 1.2
536 M HCl, with the final ~1 mL allowed to sit in the filter for ~2 hours before rinsing with 40 mL of
537 UPW and flushing with laminar flow filtered air to dry. The 0.02 µm filters were cleaned by
538 passing 20 mL of 0.02 M HCl, followed immediately by 20 mL of UPW and clean laminar flow
539 filtered air to dry.

540
541 Bulk water samples were collected in 1000 mL LDPE bottles (Nalgene®), from a 10 L Niskin
542 bottle in a field chemistry laboratory at the SLM drill site. At SLM water samples from the were
543 decanted into a 250ml LDPE bottle inside a laminar flow hood. The laminar flow hood was lined
544 with polyethylene sheeting, that had been wiped with 1 M HCl followed by 3 x wipes with
545 UPW, and the sample was decanted via gravity feed through 1 M HCl rinsed silicone tubing.
546 Approximately 1-2 L of lake water from the Niskin bottle was flushed through the tubing before
547 collection of the TE sample. Personnel conducting the sample decanting and filtration wore full
548 Tyvek clean room suits and polyethylene gloves. Bulk water samples at LG were collected from
549 a fast-moving section at the side of the main proglacial river approximately 2 km downstream of
550 the glacier portal (Fig. 1)(23) into 250 mL LDPE bottles (Nalgene®; triple rinsed with bulk
551 sample water) zip-lock bagged and taken immediately to a designated “clean” lab tent. Filtration
552 was performed within a lab made filtration box at LG, a large polypropylene box with one face
553 removed and replaced with LDPE sheeting that was taped to the box in between use, thus
554 minimizing potential contamination by dust.

555
556 Bulk samples were filtered through the 0.45 μm syringe filter (12 mL to waste/rinse, with final
557 10 mL collected), and then through a stack of 0.45 μm /0.02 μm syringe filters (12 mL to
558 waste/rinse with final 10 mL collected). Samples were additionally filtered through the 0.22 μm
559 syringe filters at SLM (12 mL to waste with final 10 mL collected). Samples were preserved in
560 the field at LG by acidifying with OptimaTM HNO_3 to a pH <2. Samples for TE from SLM were
561 collected from casts 1-3 and acidified with twice lab distilled ultra-trace metal grade HNO_3 ~3
562 months after collection, in a Class 100 clean lab and left acidified at room temperature for 6
563 weeks before analysis. Field blanks for LG were processed in the field with transported UPW
564 identically to samples. Niskin bottle blanks were prepared in the Crary Laboratory, McMurdo
565 Station, Antarctica, before field deployment at SLM. A 10 L Niskin was filled with UPW, left to
566 sit for ~30 minutes then processed as per samples.

567
568 A common concern with TE is contamination during sampling, especially when new sampling
569 methods are used (as at SLM). We are confident that hot water drilling introduced minimal
570 contamination at SLM. First, the water level in the borehole was reduced to lower the head
571 pressure in the borehole. Back pressuring the borehole in this manner allowed the lake water to
572 rise upward of 14 m into the borehole after breakthrough, avoiding potential contamination of
573 the lake by drill water entering the lake water cavity. Specific conductivity and temperature
574 profiles from a CTD cast into the lake after drilling, but prior to water sampling, showed no
575 evidence for drill water incursion into the 15 m deep lake (99). Second, much of the water in the
576 borehole originates from melting of the ice sheet side wall, not hot water injected into the
577 borehole from the drill. Procedural blanks taken from a an access port on the hot water drilling

578 system of the borehole return water (Port 9, (18)) were very low compared to measured values
579 from the lake water (Table S3), with the exception of Zn, where blanks were ~40 nM (i.e. 55 %
580 of the dZn value at SLM). Finally, the Niskin bottle was slowly lowered to mid-depth in the lake
581 water column (lake water column = 15 m deep), hence, the bottle passed through ~7.5 m of lake
582 water flushing it more than 8 volumes of lake water before samples were collected.

583

584 **4.2.2 TE analytical procedures**

585 SLM samples were measured on a Thermo Scientific™ Element 2™ HR-ICP-MS (high
586 resolution inductively coupled mass spectrometer), and LG samples were measured on a Thermo
587 Scientific™ XSERIES 2 quadrupole ICP-MS with collision/reaction cell. Be, In and Re were
588 used as internal standards to correct for drift and matrix effects (only In was used for SLM
589 samples), and eight multi-element external calibration solutions were made gravimetrically to
590 match the concentration range observed in samples. Measurement accuracy and precision were
591 checked against reference material NIST1643 (SLM), SLRS-5 (LG) or SLRS-6 (SLM; National
592 Research Council of Canada) and replicate intermediate standards. Analytical precision ranged
593 from ± 0.7 % to ± 8.9 % based on replicates of the SLRS-5 and a gravimetrically weighed
594 intermediate standard ($n = 6$ per run; Table S4), and ± 0.5 to ± 7.9 % based on replicates of
595 SLRS-6 ($n = 5$ per run; Table S5). There were two outliers to this; with Cd and Zn difficult to
596 quantify in LG samples, where precision was $> \pm 25$ % due to the low concentrations and counts
597 per second (at or close to the instrumental detection limit). Accuracy was better than ± 10 % for
598 all elements apart from Cd (LG and SLM) and Zn (LG) as detailed in Table S4 and S5.

599

600 **4.2.3 Aqueous geochemical sampling, processing and analysis**

601 The determination of pH, specific conductivity (SC), oxygen, major ion chemistry, dissolved
602 organic carbon (DOC) concentration and suspended sediment concentration (SSC) for samples
603 from LG has been previously described (42, 49, 56). Aqueous geochemical parameters were
604 measured on samples from SLM as follows; pH, casts 2, 3, SPC and major ion chemistry, casts
605 1-6, DOC, dissolved inorganic carbon (DIC) and alkalinity, casts 1-3, 5, 6, SSC, cast 1. pH was
606 measured using an Accumet™ pH electrode, connected to an Accumet™ AB15 pH meter with
607 internal temperature compensation, standardized with Orion™ Pure Water™ pH buffers
608 immediately prior to sample measurement. Additional verification of pH was conducted with the
609 CO2sys software (Excel version 1.02) using measured DIC and alkalinity and the freshwater
610 option (salinity = 0) for dissociation constants of carbonic acid (100). Specific conductivity (at
611 25 °C) was measured using a YSI 3200 conductivity probe connected to a YSI Model 3100
612 conductivity meter calibrated immediately prior to sample measurement. Samples for major ion
613 chemistry were vacuum filtered through 0.4 µm Nuclepore™ membranes into clean 60 ml HDPE
614 bottles, pre-rinsed with filtered sample and stored frozen until analysis. Major ion concentrations
615 were determined on a Metrohm 930 Compact IC Flex ion chromatograph using Metrosep C4
616 cation and A SUPP 5 anion columns (38). Suspended sediment concentration was determined
617 gravimetrically using a pre-weighed Nuclepore™ membrane, after drying at 40°C for 16 hours.
618 Alkalinity was measured by acid neutralization to pH 4.5, using bromocresol green-methyl red
619 indicator powder pillows (Permachem® reagent 94399) to detect the endpoint. A micro-pipette
620 was used to dispense µl volumes of 0.16 N H₂SO₄ into a ~25 ml lake water sample. Volumes of
621 acid and lakewater were determined gravimetrically. DIC was measured by infrared gas analysis
622 of acid sparged sub-samples from aliquots collected in gas tight serum vials. Samples for
623 determination of DOC concentrations were filtered, stored and analyzed as described in (15).

624 Oxygen concentrations were measured using a modified Winkler titration (Limnological
625 Methods for the McMurdo Long Term Ecological Research Program; (101)).

626

627 **Acknowledgements**

628 This research is part of a European Commission Horizon 2020 Marie Skłodowska-Curie Actions
629 fellowship ICICLES (grant agreement #793962) to JRH. Antarctic work was funded under the
630 Subglacial Antarctic Lakes Scientific Access (SALSA) project through U.S. NSF grants
631 1543537 to JCP, JED and MLS, and 1543453 to WBL. AS was supported by a NASA NESSF
632 fellowship (80NSSC18K1266). The Greenland research was funded by a U.K. NERC Standard
633 Grant (NE/I008845/1) to JLW and MT, a Leverhulme Trust Research Grant (RPG-2016-439) to
634 JLW, and a Royal Society Wolfson Merit Award to JLW. The authors thank all those involved
635 with fieldwork at Leverett camp and the SALSA project. We also thank A. Chiuchiolo for
636 conducting dissolved inorganic carbon analysis for SALSA, and analytical support from Dr. M.
637 Cooper at the National Oceanography Centre, U.K., Plasma Mass Spectrometry Lab, and G.
638 White in the geochemistry group at the National High Magnetic Field Geochemistry Laboratory,
639 which is supported by NSF DMR-1644779 and the State of Florida. We are extremely grateful
640 for the comments and input from T. Vick-Majors, R. Venturelli and G. Lamarche-Gagnon on an
641 earlier draft of the manuscript. The SALSA Science Team consists of T. Campbell, B. Christner,
642 C. Davis, H. Fricker, D. Harwood, A. Leventer, W. Li, A. Michaud, M. Patterson, B. Rosenheim,
643 M. Siegfried, R. Venturelli and T. Vick-Majors.

644

645 **Author contributions**

646 JRH, MLS, JLW and JCP conceived the project. JRH, MLS, JCP, JEH, CBG, TJK, MS, EAB,
647 JB, JED and MT performed the fieldwork, collected samples and undertook field measurements.
648 JRH, PLM, AS, JED, JB and MT undertook the geochemical analyses. JCP, MLS, JED, JLW,
649 MT, WBL, RGMS and JRH funded the research. JRH analyzed the data and wrote the
650 manuscript with significant input from MLS, JLW, JCP, MT and RGMS, and contributions from
651 all other co-authors.

652

653 **Competing statement**

654 The authors declare no competing interests.

655

656

657 REFERENCES CITED

- 658 1. J. L. Wadham *et al.*, Ice sheets matter for the global carbon cycle. *Nat. Commun.* **10**,
659 3567-3567 (2019).
- 660 2. J. L. Bamber, R. M. Westaway, B. Marzeion, B. Wouters, The land ice contribution to
661 sea level during the satellite era. *Environ Res Lett* **13**, 063008 (2018).
- 662 3. B. Smith *et al.*, Pervasive ice sheet mass loss reflects competing ocean and atmosphere
663 processes. *Science* 10.1126/science.aaz5845, eaaz5845 (2020).
- 664 4. D. W. Ashmore, R. G. Bingham, Antarctic subglacial hydrology: current knowledge and
665 future challenges. *Antarct Sci* **26**, 758-773 (2014).
- 666 5. M. J. Siegert, N. Ross, A. M. Le Brocq, Recent advances in understanding Antarctic
667 subglacial lakes and hydrology. *Philosophical Transactions of the Royal Society of*
668 *London A: Mathematical, Physical and Engineering Sciences* **374** (2016).
- 669 6. J. S. Bowling, S. J. Livingstone, A. J. Sole, W. Chu, Distribution and dynamics of
670 Greenland subglacial lakes. *Nat. Commun.* **10**, 2810 (2019).
- 671 7. S. P. Carter, H. A. Fricker, The supply of subglacial meltwater to the grounding line of
672 the Siple Coast, West Antarctica. *Ann Glaciol* **53**, 267-280 (2012).
- 673 8. J. C. Priscu *et al.*, "Antarctic subglacial water: origin, evolution, and ecology" in Polar
674 Lakes and Rivers, W. F. Vincent, J. Laybourn-Parry, Eds. (Oxford University Press,
675 Oxford, 2008), vol. 1, pp. 119-137.
- 676 9. A. Urrea *et al.*, Weathering Dynamics Under Contrasting Greenland Ice Sheet
677 Catchments. *Frontiers in Earth Science* **7** (2019).
- 678 10. M. Sharp, M. Tranter, Glacier biogeochemistry. *Geochem. Perspect.*
679 10.7185/geochempersp.6.2 (2017).
- 680 11. T. Cowton, P. Nienow, I. Bartholomew, A. Sole, D. Mair, Rapid erosion beneath the
681 Greenland ice sheet. *Geology* **40**, 343-346 (2012).
- 682 12. M. Tranter, J. L. Wadham, "Geochemical Weathering in Glacial and Proglacial
683 Environments" in Treatise on Geochemistry (Second Edition), H. D. Turekian, K. K.
684 Holland, Eds. (Elsevier, Oxford, 2014), [http://dx.doi.org/10.1016/B978-0-08-095975-](http://dx.doi.org/10.1016/B978-0-08-095975-7.00505-2)
685 [7.00505-2](http://dx.doi.org/10.1016/B978-0-08-095975-7.00505-2), pp. 157-173.
- 686 13. J. R. Hawkings *et al.*, The effect of warming climate on nutrient and solute export from
687 the Greenland Ice Sheet. *Geochem. Perspect. Lett.* **1**, 94-104 (2015).
- 688 14. E. Hood, T. J. Battin, J. Fellman, S. O'Neel, R. G. M. Spencer, Storage and release of
689 organic carbon from glaciers and ice sheets. *Nat. Geosci.* **8**, 91-96 (2015).
- 690 15. T. J. Vick-Majors *et al.*, Biogeochemical Connectivity Between Freshwater Ecosystems
691 beneath the West Antarctic Ice Sheet and the Sub-Ice Marine Environment. *Global*
692 *Biogeochem. Cy.* **34**, e2019GB006446 (2020).
- 693 16. J. C. Yde, N. T. Knudsen, B. Hasholt, A. B. Mikkelsen, Meltwater chemistry and solute
694 export from a Greenland Ice Sheet catchment, Watson River, West Greenland. *J Hydrol*
695 **519, Part B**, 2165-2179 (2014).
- 696 17. J. C. Priscu *et al.*, A microbiologically clean strategy for access to the Whillans Ice
697 Stream subglacial environment. *Antarct Sci* **25**, 637-647 (2013).
- 698 18. A. B. Michaud *et al.*, Environmentally clean access to Antarctic subglacial aquatic
699 environments. *Antarct Sci* 10.1017/S0954102020000231, 1-12 (2020).

- 700 19. M. J. Hopwood *et al.*, Review article: How does glacier discharge affect marine
701 biogeochemistry and primary production in the Arctic? *Cryosphere* **14**, 1347-1383
702 (2020).
- 703 20. A. C. Mitchell, G. H. Brown, Diurnal hydrological – physicochemical controls and
704 sampling methods for minor and trace elements in an Alpine glacial hydrological system.
705 *J Hydrol* **332**, 123-143 (2007).
- 706 21. S. M. Aciego, E. I. Stevenson, C. A. Arendt, Climate versus geological controls on
707 glacial meltwater micronutrient production in southern Greenland. *Earth. Planet. Sc. Lett.*
708 **424**, 51-58 (2015).
- 709 22. J. Gaillardet, J. Viers, B. Dupre, "Trace Elements in River Waters" in Treatise on
710 Geochemistry, J. I. Drever, Ed. (Elsevier, 2014), vol. 5.
- 711 23. J. R. Hawkings *et al.*, Ice sheets as a significant source of highly reactive nanoparticulate
712 iron to the oceans. *Nat. Commun.* **5** (2014).
- 713 24. C. B. Gardner *et al.*, Molybdenum, vanadium, and uranium weathering in small
714 mountainous rivers and rivers draining high-standing islands. *Geochim. Cosmochim. Acta*
715 **219**, 22-43 (2017).
- 716 25. A. M. Shiller, L. Mao, Dissolved vanadium in rivers: effects of silicate weathering.
717 *Chem. Geol.* **165**, 13-22 (2000).
- 718 26. C. A. Miller, B. Peucker-Ehrenbrink, B. D. Walker, F. Marcantonio, Re-assessing the
719 surface cycling of molybdenum and rhenium. *Geochim. Cosmochim. Acta* **75**, 7146-7179
720 (2011).
- 721 27. J. T. Cullen, M. T. Maldonado, "Biogeochemistry of Cadmium and Its Release to the
722 Environment" in Cadmium: From Toxicity to Essentiality, A. Sigel, H. Sigel, R. K. O.
723 Sigel, Eds. (Springer Netherlands, Dordrecht, 2013), 10.1007/978-94-007-5179-8_2, pp.
724 31-62.
- 725 28. A. M. Shiller, Dissolved trace elements in the Mississippi River: Seasonal, interannual,
726 and decadal variability. *Geochim. Cosmochim. Acta* **61**, 4321-4330 (1997).
- 727 29. M. M. Benjamin, J. O. Leckie, Multiple-site adsorption of Cd, Cu, Zn, and Pb on
728 amorphous iron oxyhydroxide. *J Colloid Interf Sci* **79**, 209-221 (1981).
- 729 30. M. R. Palmer, J. M. Edmond, Uranium in river water. *Geochim. Cosmochim. Acta* **57**,
730 4947-4955 (1993).
- 731 31. M. R. Palmer, J. M. Edmond, The strontium isotope budget of the modern ocean. *Earth.*
732 *Planet. Sc. Lett.* **92**, 11-26 (1989).
- 733 32. F. M. M. Morel, A. J. Milligan, M. A. Saito, "8.5 - Marine Bioinorganic Chemistry: The
734 Role of Trace Metals in the Oceanic Cycles of Major Nutrients" in Treatise on
735 Geochemistry (Second Edition), H. D. Holland, K. K. Turekian, Eds. (Elsevier, Oxford,
736 2014), <https://doi.org/10.1016/B978-0-08-095975-7.00605-7>, pp. 123-150.
- 737 33. M. C. Lohan, A. Tagliabue, Oceanic Micronutrients: Trace Metals that are Essential for
738 Marine Life. *Elements* **14**, 385-390 (2018).
- 739 34. B. S. Twining, S. B. Baines, The Trace Metal Composition of Marine Phytoplankton.
740 *Annu Rev Mar Sci* **5**, 191-215 (2013).
- 741 35. C. M. Moore *et al.*, Processes and patterns of oceanic nutrient limitation. *Nat. Geosci.* **6**,
742 701-710 (2013).
- 743 36. T. M. Downs, M. Schallenberg, C. W. Burns, Responses of lake phytoplankton to
744 micronutrient enrichment: a study in two New Zealand lakes and an analysis of published
745 data. *Aquat Sci* **70**, 347-360 (2008).

- 746 37. J. A. Graly, N. F. Humphrey, C. M. Landowski, J. T. Harper, Chemical weathering under
747 the Greenland Ice Sheet. *Geology* **42**, 551-554 (2014).
- 748 38. A. B. Michaud *et al.*, Solute sources and geochemical processes in Subglacial Lake
749 Whillans, West Antarctica. *Geology* **44**, 347-350 (2016).
- 750 39. J. R. Hawkings *et al.*, Biolabile ferrous iron bearing nanoparticles in glacial sediments.
751 *Earth. Planet. Sc. Lett.* **493**, 92-101 (2018).
- 752 40. R. Raiswell *et al.*, Iron in Glacial Systems: Speciation, Reactivity, Freezing Behavior,
753 and Alteration During Transport. *Frontiers in Earth Science* **6** (2018).
- 754 41. M. R. Siegfried, H. A. Fricker, Thirteen years of subglacial lake activity in Antarctica
755 from multi-mission satellite altimetry. *Ann Glaciol* **59**, 42-55 (2018).
- 756 42. J. E. Hatton *et al.*, Investigation of subglacial weathering under the Greenland Ice Sheet
757 using silicon isotopes. *Geochim. Cosmochim. Acta* **247**, 191-206 (2019).
- 758 43. J. R. Hawkings *et al.*, Ice sheets as a missing source of silica to the polar oceans. *Nat.*
759 *Commun.* **8**, 14198 (2017).
- 760 44. H. H. Durr, M. Meybeck, J. Hartmann, G. G. Laruelle, V. Roubex, Global spatial
761 distribution of natural riverine silica inputs to the coastal zone. *Biogeosciences* **8**, 597-
762 620 (2011).
- 763 45. R. L. Rudnick, S. Gao, "Composition of the Continental Crust" in Treatise on
764 Geochemistry (Second Edition), H. D. Holland, K. K. Turekian, Eds. (Elsevier, Oxford,
765 2014), <http://dx.doi.org/10.1016/B978-0-08-095975-7.00301-6>, pp. 1-51.
- 766 46. J. L. Wadham *et al.*, Biogeochemical weathering under ice: Size matters. *Global*
767 *Biogeochem. Cy.* **24**, GB3025 (2010).
- 768 47. R. S. Hindshaw, J. Rickli, J. Leuthold, J. Wadham, B. Bourdon, Identifying weathering
769 sources and processes in an outlet glacier of the Greenland Ice Sheet using Ca and Sr
770 isotope ratios. *Geochim. Cosmochim. Acta* **145**, 50-71 (2014).
- 771 48. E. I. Stevenson, M. S. Fantle, S. B. Das, H. M. Williams, S. M. Aciego, The iron isotopic
772 composition of subglacial streams draining the Greenland ice sheet. *Geochim.*
773 *Cosmochim. Acta* **213**, 237-254 (2017).
- 774 49. A. M. Kellerman *et al.*, Glacier Outflow Dissolved Organic Matter as a Window Into
775 Seasonally Changing Carbon Sources: Leverett Glacier, Greenland. *Journal of*
776 *Geophysical Research: Biogeosciences* **125**, e2019JG005161 (2020).
- 777 50. V. Barrón, J. Torrent (2013) Iron, manganese and aluminium oxides and oxyhydroxides.
778 in *Minerals at the Nanoscale*, eds F. Nieto, K. J. T. Livi, R. Oberti (Mineralogical
779 Society of Great Britain and Ireland), p 0.
- 780 51. G. Olivie-Lauquet, T. Allard, J. Bertaux, J.-P. Muller, Crystal chemistry of suspended
781 matter in a tropical hydrosystem, Nyong basin (Cameroon, Africa). *Chem. Geol.* **170**,
782 113-131 (2000).
- 783 52. J. P. Stegemeier, B. C. Reinsch, C. J. Lentini, J. G. Dale, C. S. Kim, Aggregation of
784 nanoscale iron oxyhydroxides and corresponding effects on metal uptake, retention, and
785 speciation: II. Temperature and time. *Geochim. Cosmochim. Acta* **148**, 113-129 (2015).
- 786 53. J. G. Dale, J. P. Stegemeier, C. S. Kim, Aggregation of nanoscale iron oxyhydroxides and
787 corresponding effects on metal uptake, retention, and speciation: I. Ionic-strength and pH.
788 *Geochim. Cosmochim. Acta* **148**, 100-112 (2015).
- 789 54. M. F. Hochella *et al.*, Nanominerals, Mineral Nanoparticles, and Earth Systems. *Science*
790 **319**, 1631 (2008).

- 791 55. H. Pryer *et al.*, Glacial Cover Affects Silicon and Iron Exports from Rivers in Chilean
792 Patagonia. *Global Biogeochem. Cy.* (in review).
- 793 56. A. D. Beaton *et al.*, High-Resolution in Situ Measurement of Nitrate in Runoff from the
794 Greenland Ice Sheet. *Environ Sci Technol* **51**, 12518-12527 (2017).
- 795 57. J. Wadham *et al.*, The potential role of the Antarctic Ice Sheet in global biogeochemical
796 cycles. *Earth Env Sci T R So* **104**, 55-67 (2013).
- 797 58. K.-U. Ulrich, A. Rossberg, H. Foerstendorf, H. Zänker, A. C. Scheinost, Molecular
798 characterization of uranium(VI) sorption complexes on iron(III)-rich acid mine water
799 colloids. *Geochim. Cosmochim. Acta* **70**, 5469-5487 (2006).
- 800 59. S. J. Markich, Uranium Speciation and Bioavailability in Aquatic Systems: An Overview.
801 *TheScientificWorldJOURNAL* **2**, 756147 (2002).
- 802 60. K. Saeki, S.-I. Wada, M. Shibata, Ca²⁺-Fe²⁺ and Ca²⁺-Mn²⁺ exchange selectivity of
803 kaolinite, montmorillonite, and illite. *Soil Sci* **169**, 125-132 (2004).
- 804 61. D. M. Chandler *et al.*, Evolution of the subglacial drainage system beneath the Greenland
805 Ice Sheet revealed by tracers. *Nat. Geosci.* **6**, 195-198 (2013).
- 806 62. G. Lamarche-Gagnon *et al.*, Greenland melt drives continuous export of methane from
807 the ice-sheet bed. *Nature* **565**, 73-77 (2019).
- 808 63. J. F. Pankow, J. J. Morgan, Kinetics for the aquatic environment - manganese. *Environ*
809 *Sci Technol* **15**, 1306-1313 (1981).
- 810 64. R. D. Cody, Adsorption and the reliability of trace elements as environment indicators for
811 shales. *J Sediment Res* **41**, 461-471 (1971).
- 812 65. T. J. Kohler *et al.*, Carbon dating reveals a seasonal progression in the source of
813 particulate organic carbon exported from the Greenland Ice Sheet. *Geophys. Res. Lett.* **44**,
814 6209-6217 (2017).
- 815 66. A. Tagliabue *et al.*, The Role of External Inputs and Internal Cycling in Shaping the
816 Global Ocean Cobalt Distribution: Insights From the First Cobalt Biogeochemical Model.
817 *Global Biogeochem. Cy.* **32**, 594-616 (2018).
- 818 67. M. P. Bhatia *et al.*, Greenland meltwater as a significant and potentially bioavailable
819 source of iron to the ocean. *Nat. Geosci.* **6**, 274-278 (2013).
- 820 68. P. J. Statham, M. Skidmore, M. Tranter, Inputs of glacially derived dissolved and
821 colloidal iron to the coastal ocean and implications for primary productivity. *Global*
822 *Biogeochem. Cy.* **22**, GB3013 (2008).
- 823 69. A. Hodson *et al.*, Climatically sensitive transfer of iron to maritime Antarctic ecosystems
824 by surface runoff. *Nat. Commun.* **8**, 14499 (2017).
- 825 70. P. van der Merwe *et al.*, High Lability Fe Particles Sourced From Glacial Erosion Can
826 Meet Previously Unaccounted Biological Demand: Heard Island, Southern Ocean.
827 *Frontiers in Marine Science* **6**, 332-332 (2019).
- 828 71. M. J. Hopwood *et al.*, Highly variable iron content modulates iceberg-ocean fertilisation
829 and potential carbon export. *Nat. Commun.* **10**, 5261 (2019).
- 830 72. R. Raiswell *et al.*, Potentially bioavailable iron delivery by iceberg-hosted sediments and
831 atmospheric dust to the polar oceans. *Biogeosciences* **13**, 3887-3900 (2016).
- 832 73. A. Dai, K. E. Trenberth, Estimates of freshwater discharge from continents: Latitudinal
833 and seasonal variations. *J Hydrometeorol* **3**, 660-687 (2002).
- 834 74. M. J. Hopwood *et al.*, Seasonal Changes in Fe along a Glaciated Greenlandic Fjord.
835 *Frontiers in Earth Science* **4** (2016).

- 836 75. A. W. Schroth, J. Crusius, I. Hoyer, R. Campbell, Estuarine removal of glacial iron and
837 implications for iron fluxes to the ocean. *Geophys. Res. Lett.* **41**, 3951-3958 (2014).
- 838 76. J. L. Wadham *et al.*, Sources, cycling and export of nitrogen on the Greenland Ice Sheet.
839 *Biogeosciences* **13**, 6339-6352 (2016).
- 840 77. J. Hawkings *et al.*, The Greenland Ice Sheet as a hotspot of phosphorus weathering and
841 export in the Arctic. *Global Biogeochem. Cy.* **30**, 191-210 (2016).
- 842 78. K. W. Bruland, R. Middag, M. C. Lohan, "Controls of Trace Metals in Seawater" in
843 Treatise on Geochemistry (Second Edition), H. D. Holland, K. K. Turekian, Eds.
844 (Elsevier, Oxford, 2014), <https://doi.org/10.1016/B978-0-08-095975-7.00602-1>, pp. 19-
845 51.
- 846 79. K. W. Bruland *et al.*, Factors influencing the chemistry of the near-field Columbia River
847 plume: Nitrate, silicic acid, dissolved Fe, and dissolved Mn. *Journal of Geophysical*
848 *Research: Oceans* **113** (2008).
- 849 80. L. Meire *et al.*, Marine-terminating glaciers sustain high productivity in Greenland fjords.
850 *Global Change Biol.* **23**, 5344-5357 (2017).
- 851 81. K. R. Arrigo, G. L. van Dijken, A. L. Strong, Environmental controls of marine
852 productivity hot spots around Antarctica. *Journal of Geophysical Research: Oceans*
853 10.1002/2015JC010888, n/a-n/a (2015).
- 854 82. M. van Hulst *et al.*, Manganese in the west Atlantic Ocean in the context of the first
855 global ocean circulation model of manganese. *Biogeosciences* **14**, 1123-1152 (2017).
- 856 83. C. Richon, A. Tagliabue, Insights Into the Major Processes Driving the Global
857 Distribution of Copper in the Ocean From a Global Model. *Global Biogeochem. Cy.* **33**,
858 1594-1610 (2019).
- 859 84. J. H. Martin, S. E. Fitzwater, R. M. Gordon, Iron deficiency limits phytoplankton growth
860 in Antarctic waters. *Global Biogeochem. Cy.* **4**, 5-12 (1990).
- 861 85. A. L. Annett *et al.*, Controls on dissolved and particulate iron distributions in surface
862 waters of the Western Antarctic Peninsula shelf. *Mar. Chem.*
863 <https://doi.org/10.1016/j.marchem.2017.06.004> (2017).
- 864 86. L. J. A. Gerringa *et al.*, Iron from melting glaciers fuels the phytoplankton blooms in
865 Amundsen Sea (Southern Ocean): Iron biogeochemistry. *Deep Sea Res Part II Top Stud*
866 *Oceanogr.* **71-76**, 16-31 (2012).
- 867 87. R. Death *et al.*, Antarctic ice sheet fertilises the Southern Ocean. *Biogeosciences* **11**,
868 2635-2643 (2014).
- 869 88. R. Person *et al.*, Sensitivity of ocean biogeochemistry to the iron supply from the
870 Antarctic Ice Sheet explored with a biogeochemical model. *Biogeosciences* **16**, 3583-
871 3603 (2019).
- 872 89. A. M. Shiller, Syringe Filtration Methods for Examining Dissolved and Colloidal Trace
873 Element Distributions in Remote Field Locations. *Environ Sci Technol* **37**, 3953-3957
874 (2003).
- 875 90. C. Laufkötter, A. A. Stern, J. G. John, C. A. Stock, J. P. Dunne, Glacial Iron Sources
876 Stimulate the Southern Ocean Carbon Cycle. *Geophys. Res. Lett.* **45**, 3377-313,385
877 (2018).
- 878 91. L. Herraiz-Borreguero, D. Lannuzel, P. van der Merwe, A. Treverrow, J. B. Pedro, Large
879 flux of iron from the Amery Ice Shelf marine ice to Prydz Bay, East Antarctica. *Journal*
880 *of Geophysical Research: Oceans* **121**, 6009-6020 (2016).

- 881 92. G. A. Cutter, Trace Elements in Estuarine and Coastal Waters - U.S. Studies from 1986–
882 1990. *Reviews of Geophysics* **29**, 639-644 (1991).
- 883 93. M. R. Cape, F. Straneo, N. Beaird, R. M. Bundy, M. A. Charette, Nutrient release to
884 oceans from buoyancy-driven upwelling at Greenland tidewater glaciers. *Nat. Geosci.* **12**,
885 34-39 (2019).
- 886 94. K. Kunde *et al.*, Iron Distribution in the Subtropical North Atlantic: The Pivotal Role of
887 Colloidal Iron. *Global Biogeochem. Cy.* **33**, 1532-1547 (2019).
- 888 95. S. P. Carter, H. A. Fricker, M. R. Siegfried, Evidence of rapid subglacial water piracy
889 under Whillans Ice Stream, West Antarctica. *J. Glaciol.* **59**, 1147-1162 (2013).
- 890 96. M. R. Siegfried *et al.* (2019) Anatomy of a draining subglacial lake in West Antarctica. in
891 *AGU Fall Meeting* (San Francisco, CA).
- 892 97. S. Anandakrishnan, D. D. Blankenship, R. B. Alley, P. L. Stoffa, Influence of subglacial
893 geology on the position of a West Antarctic ice stream from seismic observations. *Nature*
894 **394**, 62-65 (1998).
- 895 98. N. Henriksen, A. K. Higgins, F. Kalsbeek, T. C. R. Pulvertaft, Greenland from Archaean
896 to Quaternary Descriptive text to the 1995 Geological map of Greenland, 1:2 500 000.
897 2nd edition. *Geol Surv Den Greenl*, 9-116 (2009).
- 898 99. J. Priscu *et al.*, Scientific Access into Mercer Subglacial Lake: Scientific Objectives,
899 Drilling Operations and Initial Observations. *Ann Glaciol* (in review).
- 900 100. D. Pierrot, E. Lewis, D. W. R. Wallace (2006) MS Excel program developed for CO2
901 system calculations. (ORNL/CDIAC-105, Carbon Dioxide Information Analysis Center,
902 Oak Ridge National Laboratory, U.S. Department of Energy, Oak Ridge, TN.).
- 903 101. J. H. Carpenter, THE CHESAPEAKE BAY INSTITUTE TECHNIQUE FOR THE
904 WINKLER DISSOLVED OXYGEN METHOD. *Limnol. Oceanogr.* **10**, 141-143 (1965).
- 905 102. F. Pattyn, Antarctic subglacial conditions inferred from a hybrid ice sheet/ice stream
906 model. *Earth. Planet. Sc. Lett.* **295**, 451-461 (2010).
- 907 103. A. Le Brocq *et al.*, Evidence from ice shelves for channelized meltwater flow beneath the
908 Antarctic Ice Sheet. *Nat. Geosci.* **6**, 945-948 (2013).
- 909 104. J. M. Martin, M. Meybeck, Elemental Mass-Balance of Material Carried by Major World
910 Rivers. *Mar. Chem.* **7**, 173-206 (1979).
- 911

912 **Table 1:** Estimates of annual fluxes of size fractionated TEs from the Greenland Ice Sheet and
 913 the Antarctic Ice Sheet. Elemental fluxes are present either as Mmol (10^6 mol) or Gmol (10^9
 914 mol) per year. The mean is given in bold and estimated range/uncertainty are given in
 915 parentheses. Flux estimates are presented to 2 significant figures/decimal places.

Element/ variable	Unit	Greenland Ice Sheet ^a			Antarctic Ice Sheet ^b		
		d	cn	s	d	cn	s
Water flux	$km^3 yr^{-1}$	560 (410 – 730) ^c			65 (32.5 – 97.5) ^d		
Al	$10^9 mol yr^{-1}$	9.2 (0.14 – 77)	8.0 (0 – 74)	1.31 (0 – 5.8)	4.5 (2.1 – 7.1)	4.2 (2.1 – 6.3)	0.33 (0.15 – 0.53)
Ba	$10^6 mol yr^{-1}$	13 (1.3 – 60)	11 (0.03 – 58.4)	1.4 (0.23 – 22)	7.6 (3.6 – 12)	6.7 (3.3 – 10)	0.91 (0.33 – 1.8)
Cd	$10^6 mol yr^{-1}$	0.01 (0 – 0.05)	0 (0 – 0.02)	0.01 (0 – 0.04)	0.02 (0.01 – 0.02)	0.01 (0 – 0.01)	0 (0 – 0.01)
Co	$10^6 mol yr^{-1}$	0.86 (0.05 – 2.9)	0.79 (0 – 2.8)	0.07 (0.01 – 2.2)	0.48 (0.24 – 0.73)	0.48 (0.24 – 0.72)	0 (0 – 0)
Cr	$10^6 mol yr^{-1}$	3.4 (0.08 – 17)	3.2 (0.01 – 17)	0.13 (0.01 – 1.6)	2.2 (1.1 – 3.4)	1.5 (0.78 – 2.3)	0.68 (0.34 – 1.0)
Cu	$10^6 mol yr^{-1}$	5.9 (1.3 – 31)	4.7 (0.56 – 17)	1.2 (0.57 – 17)	2.9 (1.4 – 4.3)	2.6 (1.3 – 3.9)	0.27 (0.13 – 0.41)
Fe	$10^9 mol yr^{-1}$	1.3 (0.02 – 5.5)	1.3 (0.02 – 5.5)	0.01 (0 – 0.05)	1.4 (0.66 – 2.1)	1.4 (0.66 – 2.1)	0
Li	$10^9 mol yr^{-1}$	0.06 (0.03 – 0.23)	0.01 (0 – 0.15)	0.05 (0.03 – 0.12)	0.12 (0.06 – 0.18)	0.02 (0.01 – 0.03)	0.10 (0.05 – 0.16)
Mn	$10^6 mol yr^{-1}$	41 (9.6 – 380)	27 (0.15 – 220)	14 (2.3 – 370)	27 (13 – 41)	27 (13 – 40)	0.03 (0.01 – 0.04)
Mo	$10^6 mol yr^{-1}$	2.4 (0.78 – 8.3)	0	2.4 (0.78 – 8.3)	3.4 (1.7 – 5.2)	0	3.4 (1.7 – 5.2)
Ni	$10^6 mol yr^{-1}$	7.0 (0.48 – 14)	6.4 (0 – 13)	0.61 (0.25 – 12)	0.94 (0.47 – 1.4)	0.86 (0.43 – 1.3)	0.08 (0.04 – 0.12)
Pb	$10^6 mol yr^{-1}$	0.11 (0 – 0.49)	0.10 (0 – 0.48)	0.01 (0 – 0.02)	0.32 (0.16 – 0.48)	0.32 (0.16 – 0.48)	0
Sr	$10^9 mol yr^{-1}$	0.03 (0.02 – 0.14)	0	0.03 (0.02 – 0.14)	0.05 (0.03 – 0.08)	0	0.05 (0.03 – 0.08)
Ti	$10^6 mol yr^{-1}$	160 (2.2 – 610)	140 (1.1 – 600)	1.2 (0.51 – 3.7)	140 (65 – 210)	140 (65 – 210)	0
U	$10^6 mol yr^{-1}$	0.07 (0.02 – 0.55)	0.06 (0.02 – 0.48)	0 (0 – 0.07)	1.9 (0.95 – 2.9)	0	1.9 (0.95 – 2.9)
V	$10^6 mol yr^{-1}$	17 (1.4 – 65)	5.0 (0 – 48)	12 (1.3 – 23)	17 (8.6 – 26)	4.2 (2.1 – 6.3)	13 (6.5 – 20)
Zn	$10^6 mol yr^{-1}$	3.9 (0 – 20)	3.9 (0 – 20)	0.08 (0 – 1.5)	4.7 (2.0 – 7.9)	4.3 (2.1 – 7.2)	0.38 (0.17 – 0.63)

916

917 ^a Elemental flux estimates from GrIS are derived from the minimum, discharge-weighted mean and maximum
918 concentrations measured at LG multiplied by the modeled minimum, mean and maximum 2007-2016 ice sheet
919 meltwater discharge.

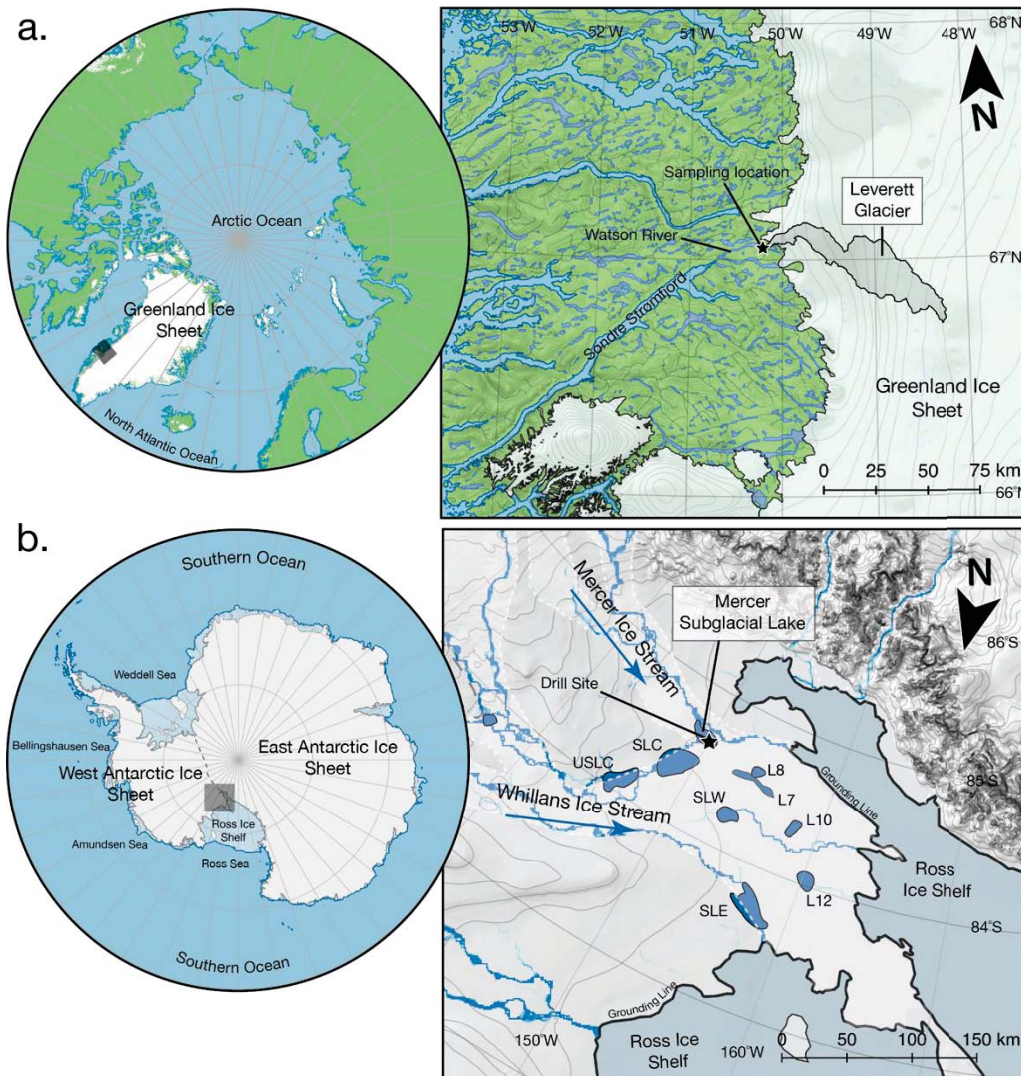
920 ^b Elemental flux estimates from AIS are derived from the minimum, mean and maximum concentrations measured
921 at SLM multiplied by the modeled minimum, mean and maximum AIS discharge.

922 ^c Mean modeled Greenland Ice Sheet meltwater discharge over 2007-2016 from (2). Min is the lowest melt year
923 (2013), max is the largest melt year (2012).

924 ^d Modeling basal melt rates from (102) with a standard deviation of $\pm 50\%$

925

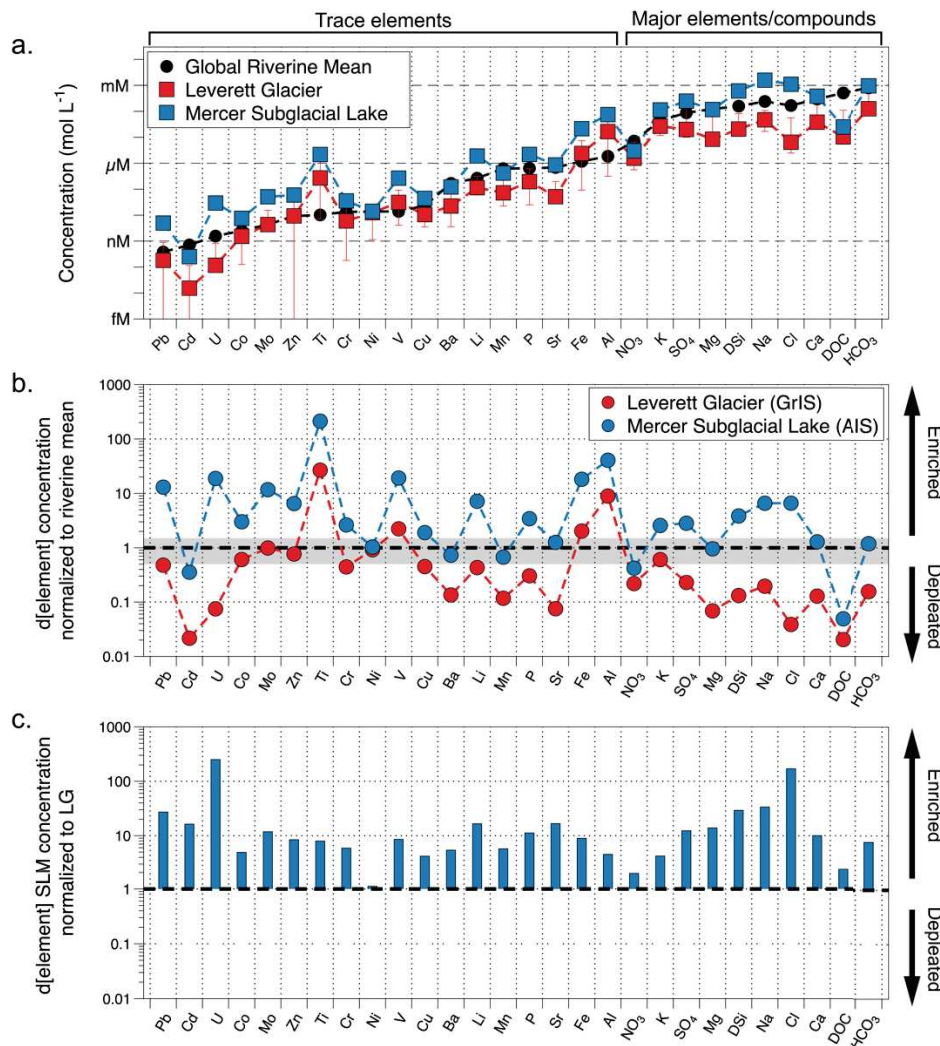
926 **Figure 1:** Map of study regions. (a) Leverett Glacier, draining the Greenland Ice Sheet, and (b)
 927 Mercer Subglacial Lake, draining the Mercer Ice Stream. Water flows into the Watson River and
 928 then Søndre Strømfjord in (a). Modeled water flow paths into the Ross Ice Shelf cavity are
 929 indicated by the blue lines in (b) (103). SLW = Whillans Subglacial Lake, SLC = Conway
 930 Subglacial Lake, USLC = Upper Conway Subglacial Lake, SLE = Engelhardt Subglacial Lake,
 931 L8...12 = Lake 8...12. Insert polar stereographic maps are cut at (a) 60°N and (b) 60°S with
 932 study areas in shaded boxes. Topographic contours of the ice sheet surface (Greenland) or bed
 933 (Antarctic) are at 100 m intervals.



934

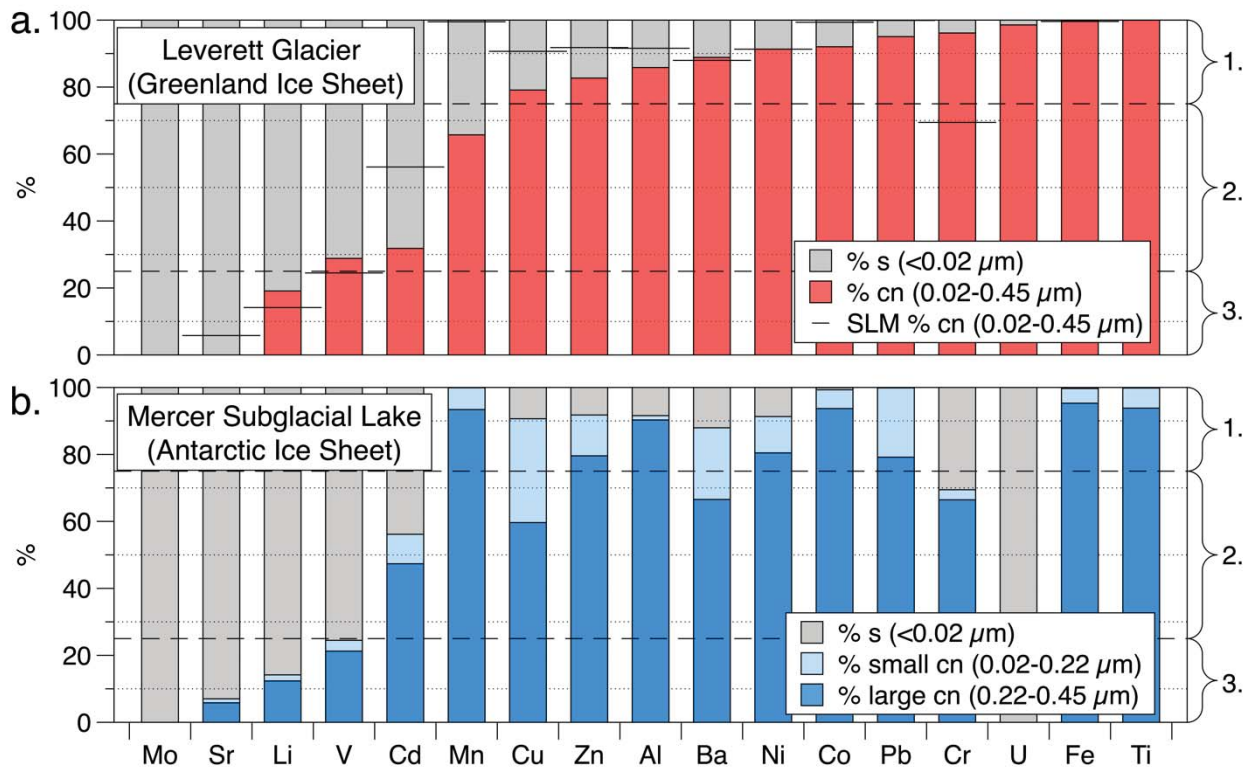
935

936 **Figure 2:** (a) Dissolved (<0.45 μm) mean elemental concentrations on a log scale in Leverett
 937 Glacier and Mercer Subglacial Lake samples, and either minimum/maximum range (Leverett
 938 Glacier) or standard deviations (Mercer Subglacial Lake), compared to best-estimate mean
 939 riverine concentrations (<0.2-0.45 μm)(22, 104). (b) Leverett Glacier and Mercer Subglacial
 940 Lake molar concentrations normalized to the global riverine mean dissolved elemental
 941 concentration (22, 104). Values of >1 equal enrichment compared to mean riverine waters.
 942 Values <1 indicate depletion compared to mean riverine waters. The grey region indicates values
 943 $\pm 50\%$ of the riverine mean. (c) Mean Mercer Subglacial Lake concentrations normalized to
 944 Leverett Glacier concentrations. Leverett Glacier DOC and major ion/Si data from (42, 49).
 945 Elements are arranged along the X-axis from lowest mean non-glacial riverine concentration to
 946 highest non-glacial mean riverine concentration. n.b., Pb, Cd and Zn minimum concentrations at
 947 Leverett Glacier are below the limit of detection.



948

949 **Figure 3:** The proportion of colloidal/nanoparticulate (cn) and soluble (s) trace element species
 950 in ice sheet meltwaters as a percentage of the <math><0.45 \mu\text{m}</math> concentration. Ordering from left to right
 951 on the x-axis is according to the percentage of the <math><0.45 \mu\text{m}</math> fraction that is filterable through a
 952 $0.02 \mu\text{m}$ pore size (i.e., our best approximation of truly dissolved species) in Greenland Ice Sheet
 953 samples with the highest on the left, and lowest on the right. Elemental groupings are indicated
 954 on the right and with the horizontal dashed lines, and are detailed in the text.
 955

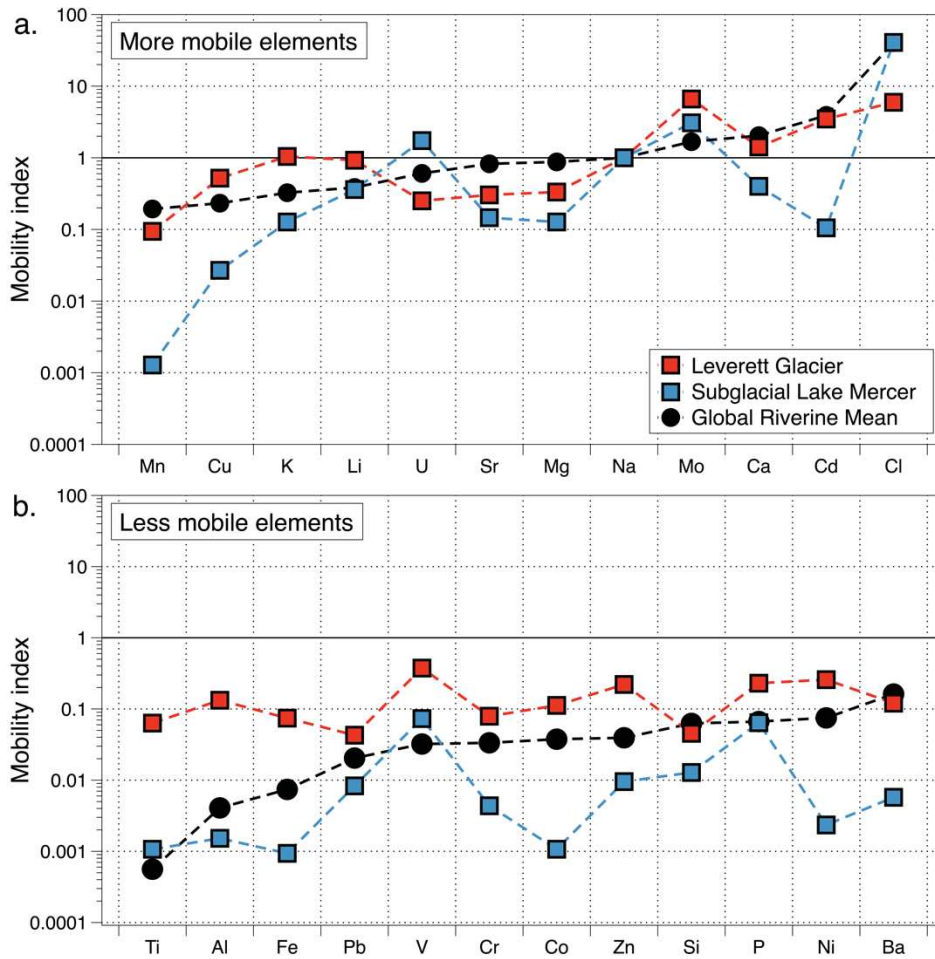


956

957

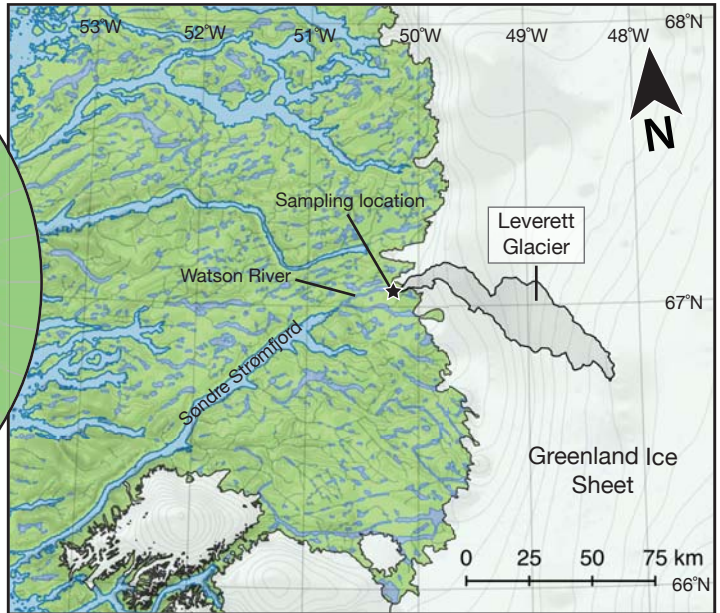
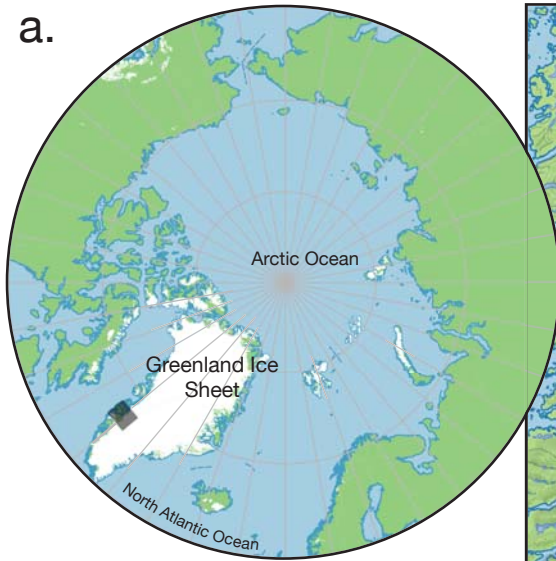
958

959 **Figure 4:** Mobility index of (a) highly mobile and (b) less mobile elements in the dissolved size
 960 fraction (<0.45 μm). Mobility index calculated via normalization of dissolved concentrations to
 961 upper continental crust abundance (22, 45, 104), with values normalized again to Na (thus Na =
 962 1 in all environments). Higher values indicate greater elemental mobility from weathering.
 963 Elements are grouped and arranged according to mean riverine mobility (22) with least to most
 964 mobile elements in the <0.45 μm size fraction going from left to right on the X-axis.
 965



966

a.



b.

